

Geophysical Research Letters



RESEARCH LETTER

10.1029/2020GL087287

The Impact of Rain on Ocean Surface Waves and Currents

Nathan J. M. Laxague¹  and Christopher J. Zappa¹ 

¹Lamont-Doherty Earth Observatory, Columbia University, Palisades, NY, USA

Key Points:

- Observations are made of the ocean surface wave and near-surface current response to a heavy rain event
- Surface gravity waves are suppressed while rain-induced ring waves dominate the sea surface
- This change in wave state results in the rapid acceleration of near-surface current

Supporting Information:

- Supporting Information S1

Correspondence to:

N. J. M. Laxague,
laxague@ldeo.columbia.edu

Citation:

Laxague, N. J. M., & Zappa, C., J (2020). The impact of rain on ocean surface waves and currents. *Geophysical Research Letters*, 47, e2020GL087287. <https://doi.org/10.1029/2020GL087287>

Received 7 OCT 2019

Accepted 11 MAR 2020

©2020. The Authors.

This is an open access article under the terms of the Creative Commons Attribution License, which permits use, distribution and reproduction in any medium, provided the original work is properly cited.

Abstract Precipitation is an important component of the interaction between Earth's atmosphere and oceans, modifying air-sea fluxes of momentum, heat, and gas. It has been hypothesized that rain's suppression of ocean surface gravity waves and centimeter-scale wave enhancement should alter the nature of air-sea momentum flux, resulting in increased near-surface current. Here, we use field observations to describe this impact and measure the very near-surface current response to rainfall. During heavy rain, surface-roughening ring waves were generated and longer gravity waves were suppressed; immediately following, the magnitude of the near-surface current increased in response to wind forcing but died as the rain subsided and long waves recovered. These first-of-their-kind field observations indicate that rain reduces ocean wave form drag in favor of tangential stress, resulting in the acceleration of current near the sea surface.

Plain Language Summary Rain is known to be an important component of atmosphere-ocean interactions. However, the specific response of short-scale waves and very near-surface current to precipitation has not yet been described in the Earth's ocean. We observe that rainfall suppresses long waves and grows centimeter-scale ring waves. This alteration facilitates the acceleration of current, which ceases in favor of longer wave growth as the rain subsides. This is the first observation of this phenomenon in the Earth's real ocean.

1. Introduction

High levels of rainfall are commonly observed over the tropical regions of Earth's oceans, impacting physical processes that influence weather and climate from the microscale to the basin scale. Rain has been shown to alter major circulation patterns (Lee et al., 2019) and stir the upper ocean (Abe et al., 2019) through the large-scale freshening of the ocean's near-surface layer. In areas which typically see low levels of wind forcing and high levels of rainfall, such as the Western Equatorial Pacific, rain has been observed to have a substantial impact on air-sea fluxes (Turk et al., 2010). It is understood that rainfall on the ocean creates a thin, highly turbulent fresh lens near the surface (Harrison & Veron, 2017; Peirson et al., 2013; Zappa et al., 2009), which enhances air-sea flux but temporarily stalls vertical mixing (Ho et al., 1997; Schlüssel et al., 1997; Zappa et al., 2009). Under low levels of wind forcing, this lens—often several meters thick—forms what is known as a “slippery layer” (Anderson et al., 1996; Kudryavtsev & Soloviev, 1990), accelerating past the saline water at the base of the lens (Shcherbina et al., 2019; Wijesekera et al., 1999). This phenomenon has been extensively studied and documented in the literature—particularly in recent years (e.g., Doeschate et al., 2019; Dong et al., 2017; Drushka et al., 2016; Volkov et al., 2019; Shcherbina et al., 2019; Thompson et al., 2019). This fresh lens is typically tens of centimeters thick, with turbulent kinetic energy dissipation falling orders of magnitude over the upper half meter of the water column (Zappa et al., 2009).

Precipitation also has a profound impact on the ocean surface wave state. Rainfall has long been known to “knock down the sea”—that is—to attenuate ocean surface gravity waves (Reynolds, 1900; Tsimplis & Thorpe, 1989). This fact is often emphasized as the key feature of the relationship between rain and ocean surface waves (Cavaleri & Bertotti, 2017; Cavaleri et al., 2015; Tsimplis & Thorpe, 1989). However, rain also generates centimeter-scale water surface undulations of its own. Under heavy rainfall, these may be the chaotic pockmarks, which result from the frequent and violent interaction between raindrops and impact craters. Under light rainfall, they may be the radially propagating features known as “ring waves.” A ring wave is characterized by an impact crater, downward and outward flow, and a rapid upward jet (Morton et al., 2000). Numerous laboratory measurements have shown that the generation of ring waves by the impact of rain on an air-water interface is substantial, especially in light wind conditions (Bliven et al., 1993, 1997; Harrison et al., 2012; Poon et al., 1992; Yang et al., 1997). Even under substantial levels of wind forcing, rain

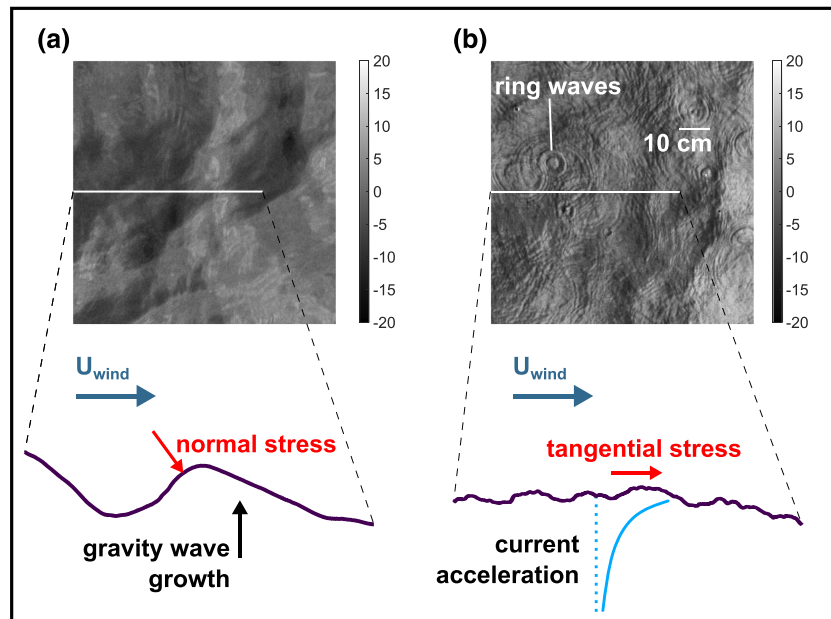


Figure 1. In this schematic, the prerain surface (slope field in (a)) features gravity waves, which take up momentum from the atmosphere via normal stress. The rain-affected surface (slope field in (b)) is characterized by ring wave-scale roughness which enhances tangential stress, feeding the near-surface current. Slope field spatial scale (the 10-cm bar) is given for reference. Violet traces indicate the to-scale water surface vertical displacement taken along the white slices on the slope fields.

is believed to play an important role in air-sea fluxes. Inclusion of the roughening effect of rain impacting the ocean surface in extreme weather forecasting has been shown to improve the ability of models to accurately describe wave height and wind speed (Katsafados et al., 2018).

Laboratory observations have shown that simulated rainfall on an air-water interface aids in the rapid downwind acceleration of near-surface current (Poon et al., 1992). This is owed to the combined effect of rainfall to attenuate ocean surface gravity waves and enhance centimeter-scale undulations, altering the nature of air-sea momentum flux (Poon et al., 1992; Schlüssel et al., 1997). Specifically, at centimeter wavelength scales, water surface undulations serve to increase the roughness in a way that increases tangential stress, enhancing near-surface current with increasing wind speed. At scales where flow sheltering becomes significant (wavelengths of order 1 m and larger), water surface undulations serve to increase the surface-normal force, enhancing wind-wave growth with increasing wind speed. This is graphically depicted in Figure 1, with a rain rate of approximately 10 mm/hr.

Despite the numerous laboratory and theoretical studies (Veron & Mieussens, 2016) in this area, the effect of rain on the ocean surface remains one of the least understood processes in air-sea interaction (Katsafados et al., 2018). This is largely due to the absence of field measurements of rain impacting ocean surface waves and very near-surface flows. Generally, analysis of the water surface wave response to rain is centered around the calculation of wave growth and attenuation rates. In the laboratory, this has been accomplished by measuring wave parameters in a wind-wave flume upstream and downstream of an artificial rainmaker; there, the variation is spatial, not temporal (Tsimplis & Thorpe, 1989; Tsimplis, 1992; Poon et al., 1992). This is in stark contrast to what happens in the real ocean, where rain-induced changes to the wave field may occur rapidly, but environmental conditions do not vary in space over nominal observational domains of order 1–10 m for prolonged periods of time. In this way, theory and the existing body of laboratory observations are not sufficient to describe the problem of rain impacting ocean surface waves and very near-surface currents. Consequently, an improved understanding of the physical interaction between rain and the air-sea interface requires in situ observations made in the real ocean.

Here we report on field observations made of the centimeter to decimeter-scale wave and near-surface responses to an impulsive rain and wind forcing event. Wind gusts are by nature transient events with potentially substantial impacts on air-sea interaction (e.g., Zappa et al., 2019). Previous studies of skin layer

physical, chemical, and biological properties based on data from the research cruise on which these measurements were made have highlighted precipitation as an area of great interest for air-sea interaction (Wurl, Bird, et al., 2018; Wurl, Landing, et al., 2018). What follows is a description of the measurements made during the precipitation event, the analysis used to interpret the observational data, and a discussion of its importance for the study of atmosphere-ocean interactions.

2. Observations and Analysis

In October–November 2016, the R/V Falkor (supporting information Figure S1) served as an air-sea interaction observational platform in the Timor Sea and Western Equatorial Pacific (Wurl, Landing, et al., 2018). During this cruise, over two hundred 20-min observations were made of short wave topography and sea surface microlayer properties, including the application of a novel near-surface current sensing technique (Laxague et al., 2017, 2018; Laxague & Zappa, 2020). Despite the prevalence of precipitation in this region of the ocean, of these measurement periods, only one contained a rain event which was substantial (rain rate R reaching 100 mm/hr) and sustained (duration greater than 5 min). At the beginning of the period of interest, the wind speed was a steady 3 m/s. Light rain began to fall after approximately 7 min, followed by a burst of wind and heavy rain seven minutes later. A time series of the observed wind speed and rain rate is shown in Figure 2a; other measurements and analysis techniques are described throughout the remainder of section 2.

2.1. Meteorological Measurements

Wind speed was measured at a sampling rate of 1 Hz using a Gill MetPak Pro 2-D sonic anemometer mounted on the foremast at 10 m above the mean water level (supporting information Figure S1c). During periods of dedicated observation, a remotely controlled catamaran was deployed. It was equipped with a Davis Instruments Vantage Pro2 weather station, enabling the measurement of rain rate R (reported once every minute in units of mm/hr). This sensor is accurate to $\pm 4\%$ of total rain rate for rates up to 50 mm/hr and $\pm 5\%$ of total rain rate for rates between 50 and 100 mm/hr. Data were obtained from the public PANGAEA archive (Wurl et al., 2017, <https://doi.org/10.1594/PANGAEA.882430>).

2.2. Wave Field Sensing and Fourier Analysis

The ocean surface wave field was measured with high spatial and temporal resolution via Polarimetric Slope Sensing (Zappa et al., 2008, 2012). This technique allowed us to obtain the water surface slope field without disturbing any of its features; it has been successfully used to make measurements of gravity-capillary wave properties in the open ocean (Laxague et al., 2015, 2018) (supporting information Figure S2). The polarimetric camera deployed on the R/V Falkor was a custom-built system designed to minimize sensor integration time (and therefore motion blur) (Zappa et al., 2012). It enclosed two polarizing beamsplitters and four JAI monochrome digital cameras (model CV-A10CLM). Each camera provided the polarized light intensity over a 768×576 pixel array at 10-bit depth and 60 frames per second. The polarimeter was mounted 11 m above the mean water level, allowing the instrument to resolve waves with spatial scales of 1 m down to 1 mm at a rate of 60 frames per second. The camera housing included an Xsens model MTi Inertial Measurement Unit, complete with onboard processing capabilities for integrating rotation rates to produce Euler angles. The MTi sampled at 100 Hz had an angular resolution of 0.05° , and a dynamic accuracy of $\pm 2.0^\circ$. The instantaneous polarimeter position and attitude were then used to rotate the camera look vector in three dimensions and project each slope field onto the free surface.

Given a set of measurements of the spatiotemporal evolution of the water surface slope field, we may compute the directional wavenumber-frequency slope spectrum $S(k_x, k_y, \omega)$ in dimensions of m^2/Hz , varying with the Cartesian wavenumbers k_x and k_y (rad/m) and radian frequency ω (rad/s). This is described in greater detail within the supporting information. For our purposes here, this spectrum functions as a condensation of the wave state and propagational characteristics. From $S(k_x, k_y, \omega)$, we obtain the dimensionless saturation spectra $B(k_x, k_y)$ and $B(k)$ and the spectral wave growth rate $\beta(k, t)$ in dimensions of s^{-1} (Plant, 1982). Key to the analysis here is the computation of these spectra over short time windows in order to describe the temporal development of wave and current characteristics (Laxague & Zappa, 2020).

In order to interpret the effects of changing wind and rain conditions on different scales of ocean surface waves, we partitioned wave regimes by dominant restoring force. Our observed parameter space spans waves restored to equilibrium solely by gravity (gravity waves) to those restored to equilibrium solely by capillarity (capillary waves) and those restored by both effects (gravity-capillary waves) (Laxague et al., 2015). These

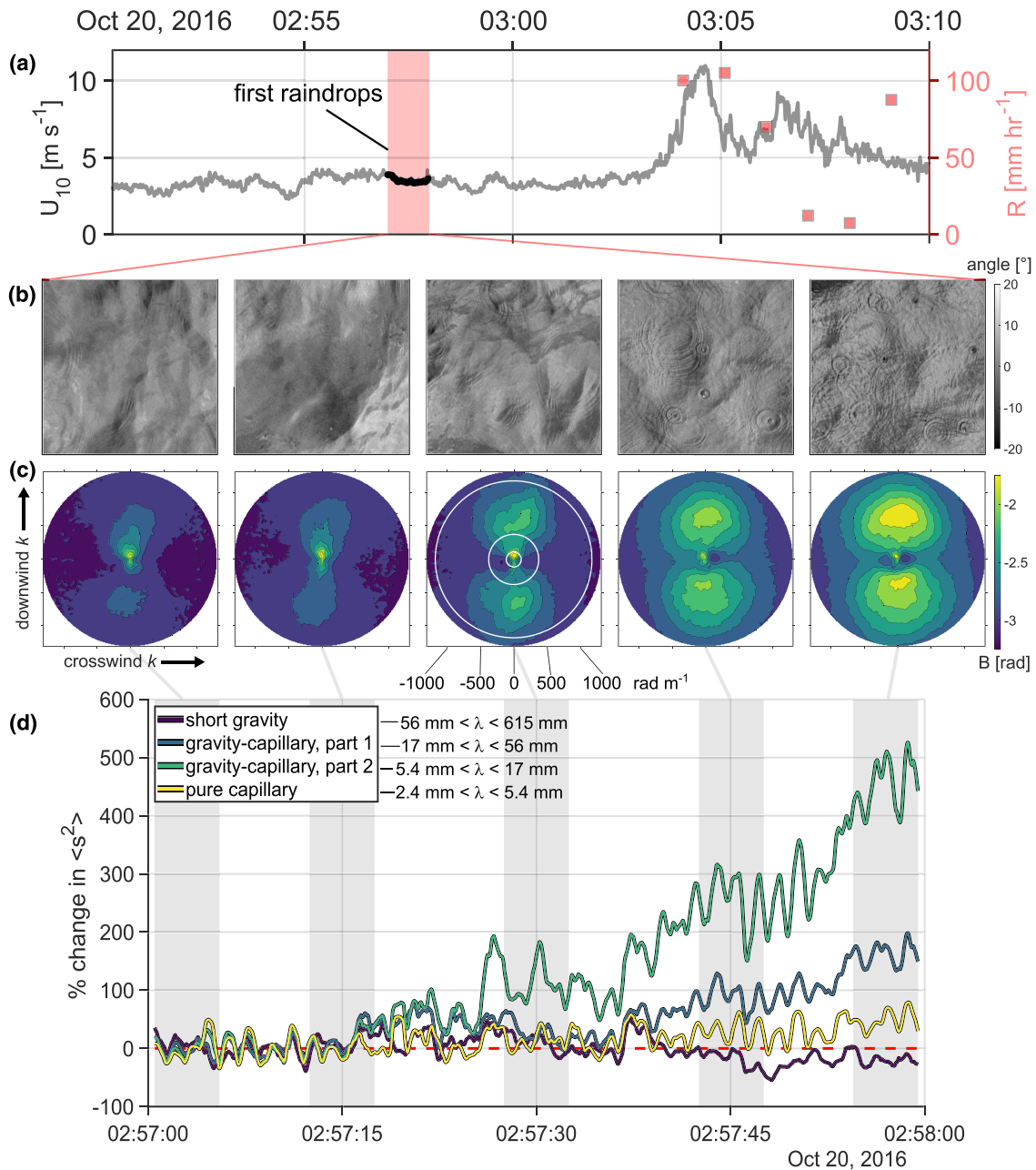


Figure 2. Graphical representation of the the first impacts of light rain on the surface wave field. (A) Gray trace: wind speed measured from bow of R/V Falkor at 10 m above mean water level; red squares: rain rate measured aboard the remote catamaran. (b) Time evolution of the ocean surface wave slope field (gray level in degrees) for wavelengths ranging between 60 cm down and 1.2 mm. (c) Corresponding directional wavenumber saturation spectra computed over 5 s, oriented in downwind direction. The white concentric rings mark the boundaries between the four wave regimes defined in section 2.2. Color indicates saturation spectral density in radians. (d) Percent change in water surface slope variance over the four chosen wave bands. Note that the gray shaded regions corresponding to Fourier transform windows of spectra shown in (c).

regimes are provided as wavelength ranges in Figure 2d and are featured on both Figures 3 and 4. They were separated by their values of the Bond number Bo (Veron & Melville, 2001):

$$Bo = \frac{\sigma k^2}{\rho g} \quad (1)$$

Here, σ is surface tension, ρ is the density of water, and g is the acceleration due to gravity. Where $Bo < 0.1$, gravity dominates; where $Bo > 10$, capillarity dominates; the range where Bo is of order 1 (gravity-capillary waves) is conveniently split into two parts, separated at $Bo = 1$. By computing ρ from shipboard in situ

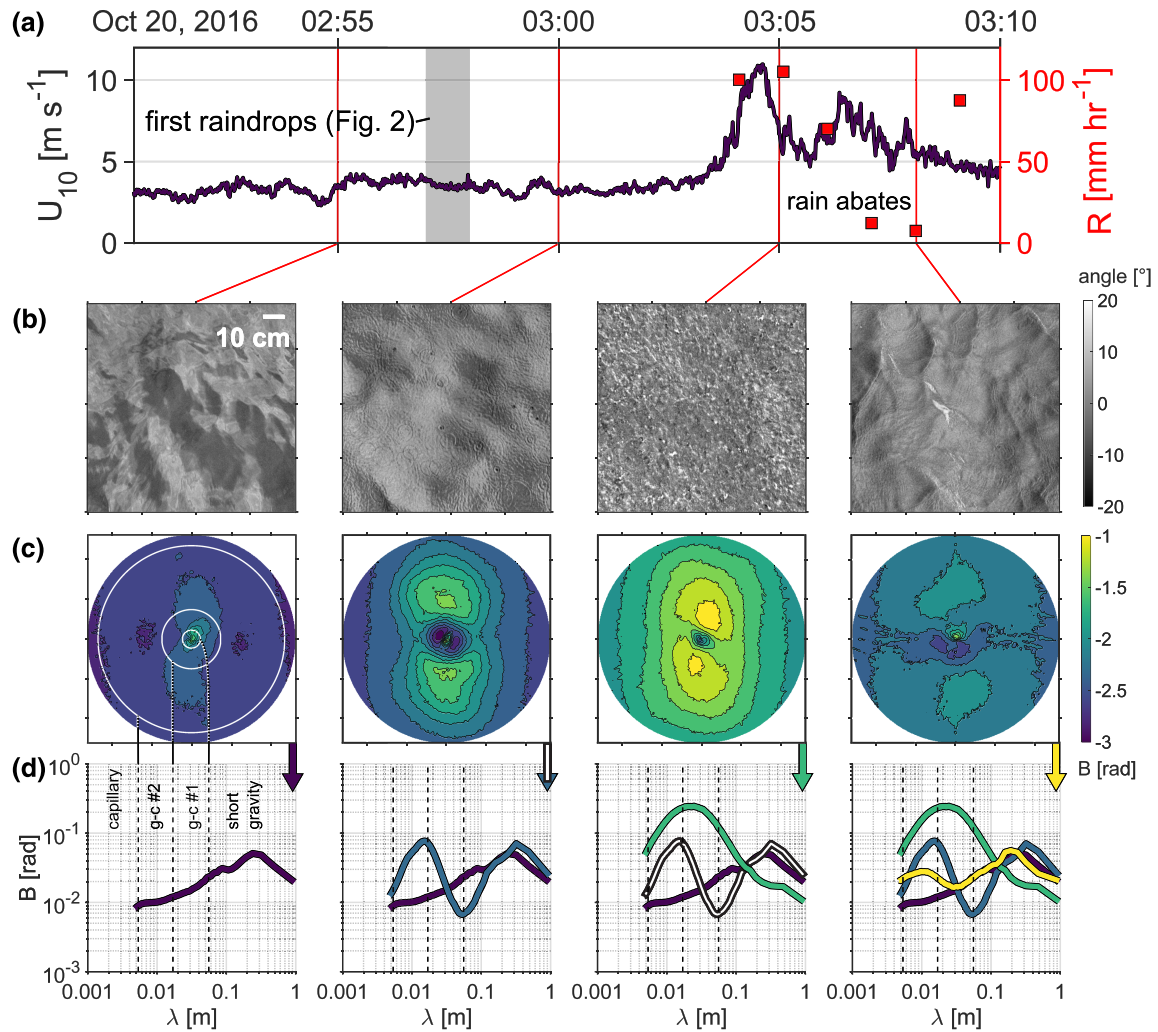


Figure 3. Selected examples of the rain event's impact on the surface wave field. (a) Dark violet trace: wind speed measured from bow of R/V Falkor at 10 m above mean water level; red squares: rain rate measured aboard the remote catamaran. Vertical red lines mark times of interest for rest of figure. (b) Along-look water surface slope field (gray level in degrees). (c) Directional wavenumber saturation spectra $B(k_x, k_y)$ computed over 5 s. Scale limits match those of Figure 2, and the white concentric rings mark the boundaries between the four wave regimes defined in section 2.2. (d) Omnidirectional saturation spectra, represented as function of wavelength λ . Trace colors correspond to the four example cases, as indicated by the vertical arrows between (c) and (d). Wavelength regimes introduced in section 2.2 are separated by vertical dashed lines.

temperature and salinity data ($1,025 \text{ kg/m}^3$) (Millero & Poisson, 1981) and taking reasonable values for σ (0.073 N/m) (Harkins & Brown, 1919) and g (9.81 m/s^2), this allows us to compute the water surface slope variance partitioned into short gravity ($k < 112.7 \text{ rad/m}$), gravity-capillary (Part 1, $112.7 < k < 371 \text{ rad/m}$; Part 2, $371 < k < 1,173 \text{ rad/m}$), and pure capillary ($k > 1,173 \text{ rad/m}$) regimes (Laxague et al., 2015, 2017).

2.3. Measurement of Near-Surface Current

The directional wavenumber-frequency spectra of short gravity waves have also been used to estimate the near-surface current (Laxague et al., 2017) (supporting information Figure S3c). Short gravity wave propagation is sensitive to currents in the upper few centimeters of the ocean surface layer, making their study quite useful for describing near-surface currents (Laxague et al., 2017). For each wavenumber-frequency spectrum, a slice was taken in the downwind direction; the $k - \omega$ coordinate pairs for peak spectral energy density were identified (supporting information Figure S3c), allowing computation of observed wave celerity $c_p = \frac{\omega}{k}$ in the upwind and downwind directions (Laxague et al., 2017, 2018; Laxague & Zappa, 2020). The difference between the upwind and downwind celerity ΔC_p retains the effect of the Doppler shift; this is $U(k)$, the current encountered by each wave component as a function of the wavenumber (Plant & Wright,

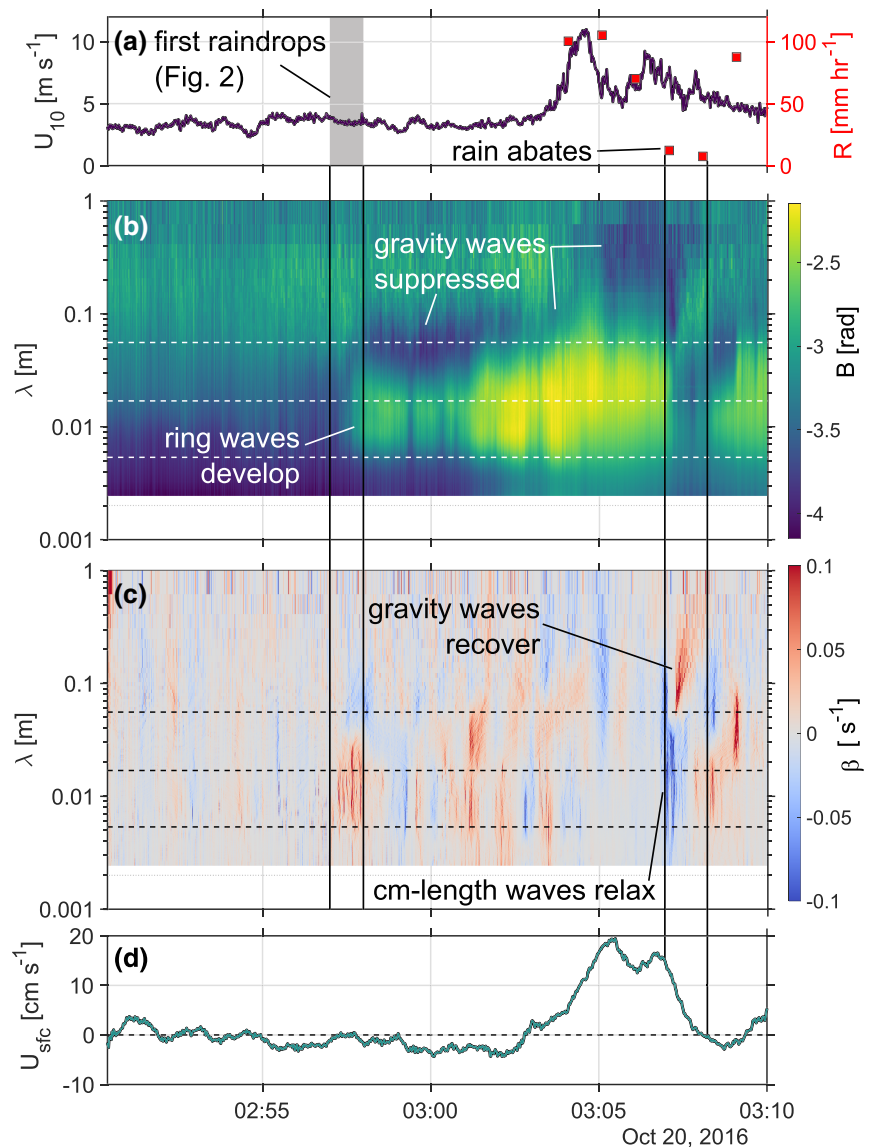


Figure 4. Time series of full rain event. (a) Dark violet trace: wind speed measured from bow of R/V Falkor at 10 m above mean water level; red squares: rain rate measured aboard the remote catamaran. (b) Surface wave saturation spectrogram in units of radians, plotted against wavelength; separations between wave regimes are marked with horizontal white dashed lines. (c) Surface wave spectral growth rate in units of s^{-1} , plotted against wavelength. (d) Near-surface ($-1.0 \text{ cm} < \zeta < -0.5 \text{ cm}$) downwind current obtained from the short wave Doppler shifts.

1980). Recent work on near-surface wave-current interaction has resulted in a new inversion technique to reliably map from $U(k)$ to a depth profile $U(z)$ (Smeltzer et al., 2019). However, the short duration and transient nature of the event described here prevented a rigorous evaluation of the variation of U with respect to k or z (Laxague & Zappa, 2020). As a result, we simply averaged $U(k)$ over the wavenumber range 25–50 rad/m, yielding the mean current between $\approx 5\text{-mm}$ and 1-cm depth (Plant & Wright, 1980), a range sufficiently “near surface” for our purposes here. The current time series shown in Figure 4d is the product of this computation. It has been subjected to a 60-s median filter to remove any residual wave motions while retaining the mean downwind flow.

3. Results and Discussion

Immediately before the rain event, the wind blew at a steady 3 m/s and short gravity waves propagated downwind with tight directional spreading (Figure 2c). Once the first raindrops were seen in the slope

field imagery—but before rainfall had become heavy enough to register on the tipping-bucket rain gauge (Figure 3a)—the directional spreading of gravity-capillary waves increased markedly as ring waves grew (Figure 2c). The dominant direction of wave propagation was observed to be downwind, though elevated levels of wave energy were found in all directions due to the isotropic nature of the ring waves. The rain impact on the sea surface also resulted in a substantial ($\approx 100\%$) increase in slope variance within the short gravity-capillary wave regime encompassing ring waves and a slight reduction in short gravity wave slope variance (Figure 2d). The omnidirectional wave spectrum shown at time 3:00 of Figure 3d reveals simultaneous wave enhancement at wavelengths of 1 mm to 5 cm and damping at wavelengths of 5–10 cm.

The arrival of the wind and rain front had a substantial effect on the observed wave state. As seen at time 3:05 of Figure 3, the impact of heavy rainfall completely dominates the ocean surface wave structure, with coherent ring waves subsumed by densely packed impact craters and jets. These features are largely isotropic, though a slight propagational tendency exists in the downwind direction. At this point, waves of length $\lambda > 20$ cm have been significantly attenuated. Another view of this transition in sea state is provided in the spectrogram of Figure 4b, where centimeter-scale waves in the middle of the gravity-capillary domain are shown to have grown substantially and the intense (≈ 100 mm/hr) rainfall resulted in the suppression of longer gravity waves. After approximately 3 min of heavy precipitation, the rain briefly subsided (for ≈ 2 min). Gravity-capillary waves relaxed substantially, as shown in the short wave spectrogram and spectral growth rate β provided in Figures 4b and 4c. This was accompanied by the substantial growth of short surface gravity waves (Figure 4c), free to develop under wind forcing without the suppressive effects of rain.

From the wind and rain front's first impact on the measurement location at time $\approx 3:04$ to the pause in rainfall seen at time $\approx 3:08$, an impulsive increase in downwind near-surface current was observed (Figure 4d). This burst of current peaked in magnitude immediately after both the wind speed and rain rate reached their observed maxima. However, 2 min later, the current magnitude rapidly fell to its preburst magnitude despite the fact that the wind speed remained elevated (7–9 m/s). It was at this point that the rain rate dropped to less than 10 mm/hr by the rain gauge's measure and ring waves became nearly imperceptible in the short wave slope fields (Figure 3d). One potential explanation for this series of events is that the rain event created a slippery layer (Kudryavtsev & Soloviev, 1990; Shcherbina et al., 2019), which allowed the impulsive wind to rapidly accelerate the near-surface flow. Once the rain had subsided, the wind forcing worked to mix the slippery layer back into the saline upper ocean, reducing the near-surface current magnitude. This explanation requires the full development and extinguishment of a slippery layer within 5 min time under high levels of wind forcing, an outcome which is unlikely based on many measurements of such layers' development (Dong et al., 2017; Doeschate et al., 2019; Thompson et al., 2019; Shcherbina et al., 2019; Volkov et al., 2019). The spectral growth rate shown in Figure 4c is likely the key to understanding this observed sequence of events. At the precise moment that the rain rate dropped and the near-surface current decelerated, rain-induced surface undulations in the gravity-capillary scale range of the spectrum relaxed. However, the wind speed remained relatively high, resulting in a growth spurt among short surface gravity waves. The wave slope field and spectra shown at time $\approx 3:08$ in Figures 3b–3d reveal a sea state that is in the midst of returning to its prerin form. It is therefore the likeliest explanation that the ocean wave state was the determining factor in the growth and subsidence of the near-surface current burst. This is in line with previous observations made in the laboratory (Poon et al., 1992) and is consistent with wind-wave theory (Schlüssel et al., 1997).

Given that the present study is focused on the results of a single field measurement of a transient phenomenon, it is difficult to extrapolate this phenomenon's importance for larger-scale processes. The effect of rain to produce a buoyant fresh lens, trapping the rain-enhanced turbulence near to the ocean surface (e.g., Harrison & Veron, 2017; Zappa et al., 2009) has been widely observed. We note that the canonical slippery layer presented by Shcherbina et al. (2019) was shown to accelerate from 0–20 cm/s over ≈ 5 hr, while the centimeter-depth current described in the present work accelerated from 0–20 cm/s over ≈ 2 min—approximately 150 times faster. In general, the latter's rate of change is likely to be strongly dependent on the initial wave state and the nature of temporal variation to the wind and rainfall conditions. Furthermore, the vertical structure of this phenomenon remains to be described in full—though it is certainly a very near-surface effect (Poon et al., 1992). Future efforts to observe the impact of rainfall on turbulence in the ocean surface layer should consider the phenomenon described in the present work in addition to the deeper and longer-developing phenomena associated with stratification and slippery layers.

As coupled wind-wave-current models (e.g., Curcic et al., 2016) become more widely used in geophysical research, there is an opportunity to incorporate rain-related effects into these modeling efforts. The Chemical Hydrological Atmospheric Ocean wave System framework allows for the parameterization of rain-induced gravity wave suppression and changes to the surface roughness length in a wind-wave coupled framework (Varlas et al., 2018). This parameterization has been shown to improve model skill in retrieving wind speed and wave height under tropical cyclone-force conditions (Katsafados et al., 2018). The phenomenon described in the present work could be reproduced in a fully coupled wind-wave-current modeling environment, provided that environment (1) allows for the parameterization of rain's impact on the ocean surface and (2) is able to partition momentum flux between form drag and tangential stress. Given the ubiquity of precipitation over Earth's oceans, accounting for these processes would positively impact the community's modeled representation of air-sea interaction.

4. Conclusions

Rain's simultaneous suppression of surface gravity waves and enhancement of short-scale, low-amplitude ring waves changes the nature of air-sea momentum flux, feeding near-surface current at the expense of wave growth. This mechanism has been described using laboratory observations (Poon et al., 1992) and is supported by both theory and physical intuition (Schlüssel et al., 1997). Here, the initial increase in near-surface current magnitude followed a similar jump in both wind and rain intensity. However, the cessation in rainfall as wind speed remained high was accompanied by simultaneous gravity-capillary wave relaxation/surface gravity wave growth and the reduction of current magnitude. Given the relative timing of changes to the measured near-surface current and the wind and rain conditions, we find the mechanism of the wave state changing the nature of momentum flux to be the best explanation for the phenomenon observed here.

At the macroscale, rain is understood to have an important impact on sea surface processes, influencing ocean circulation patterns, weather, and climate. However, numerical models rarely incorporate the effects of precipitation on air-sea transfer mechanisms—a direct consequence of our lack of understanding in this area. As these models improve in resolution and sophistication, it becomes imperative to make high quality observations of the fundamental physical phenomena underpinning the processes being modeled.

The work we describe here is such an observation, leveraging modern camera technology (Zappa et al., 2012) with novel processing (Zappa et al., 2008) and analysis (Laxague et al., 2017) techniques. We have made in situ measurements of the impact of rain on millimeter to meter-scale waves and underlying mean flow in the open ocean. Observations of the impact of rain on ocean surface waves are sparse, and none of them have elucidated the direct response of ring waves and very near-surface current to precipitation. The effect of rain to modify ocean surface wave geometry enhancing tangential stress and accelerating current in the aqueous surface layer has been hypothesized based on laboratory experiments and physical intuition (Poon et al., 1992; Schlüssel et al., 1997); our results offer the first field validation of this phenomenon.

This is a small but unique set of observations of a fundamental physical process in the open ocean. The transient nature of wind gusts and fleeting rain events make them difficult to target for in situ studies; nevertheless, further work is needed to quantify the importance of these impulsive wind and rain events with respect to regional and global air-sea interaction. We do hypothesize that these types of transient events may provide injections of energy into the aqueous surface layer, stirring the region and enhancing mixing with saltier water from below. Whether or not this particular effect is sufficiently ubiquitous to be significant in the context of weather, climate, or ocean circulation models remains to be seen. However, this work does underscore the importance of continuing to make in situ observations of fundamental physical processes as our technological capabilities advance.

References

- Abe, H., Ebuchi, N., Ueno, H., Ishiyama, H., & Matsumura, Y. (2019). Aquarius reveals eddy stirring after a heavy precipitation event in the subtropical North Pacific. *Journal of Oceanography*, 75(1), 37–50. <https://doi.org/10.1007/s10872-018-0482-0>
- Anderson, S. P., Weller, R. A., & Lukas, R. B. (1996). Surface buoyancy forcing and the mixed layer of the western Pacific warm pool: Observations and 1D model results. *Journal of Climate*, 9(12), 3056–3085. [https://doi.org/10.1175/1520-0442\(1996\)009<3056:SBFATM>2.0.CO;2](https://doi.org/10.1175/1520-0442(1996)009<3056:SBFATM>2.0.CO;2)
- Bliven, L. F., Branger, H., Sobieski, P., & Giovanangeli, J.-P. (1993). An analysis of scatterometer returns from a water surface agitated by artificial rain: Evidence that ring-waves are the main feature. *International Journal of Remote Sensing*, 14(12), 2315–2329. <https://doi.org/10.1080/01431169308954039>

Acknowledgments

The authors thank Carson Witte and Sophia Brumer for their effort in data collection and Róisín Commene for her helpful insights on the manuscript. The thorough and constructive comments provided by Mark Bourassa and two anonymous reviewers are greatly appreciated. Finally, the authors thank the captain and crew of the R/V Falkor. Observational work was supported by the Schmidt Ocean Institute as part of the AIR↓↑SEA expedition (FK161010). Analysis was supported by NSF Grant 19-23935. The observational data and MATLAB codes used in this work are publicly available through the Columbia Academic Commons (DOI: 10.7916/d8-2q9z-t618). This is Lamont-Doherty Earth Observatory Contribution 8388.

- Bliven, L. F., Sobieski, P. W., & Craeye, C. (1997). Rain generated ring-waves: Measurements and modelling for remote sensing. *International Journal of Remote Sensing*, 18(1), 221–228. <https://doi.org/10.1080/014311697219385>
- Cavaleri, L., & Bertotti, L. (2017). The attenuation of swell waves by rain. *Geophysical Research Letters*, 44, 10,504–10,510. <https://doi.org/10.1002/2017GL075458>
- Cavaleri, L., Bertotti, L., & Bidlot, J.-R. (2015). Waving in the rain. *Journal of Geophysical Research: Oceans*, 120, 3248–3260. <https://doi.org/10.1002/2014JC010348>
- Curcic, M., Chen, S. S., & Özgökmen, T. M. (2016). Hurricane-induced ocean waves and Stokes drift and their impacts on surface transport and dispersion in the Gulf of Mexico. *Geophysical Research Letters*, 43, 2773–2781. <https://doi.org/10.1002/2015GL067619>
- Doeschate, A., Sutherland, G., Bellenger, H., Landwehr, S., Esters, L., & Ward, B. (2019). Upper ocean response to rain observed from a vertical profiler. *Journal of Geophysical Research: Oceans*, 124, 3664–3681. <https://doi.org/10.1029/2018JC014060>
- Dong, S., Volkov, D., Goni, G., Lumpkin, R., & Foltz, G. R. (2017). Near-surface salinity and temperature structure observed with dual-sensor drifters in the subtropical South Pacific. *Journal of Geophysical Research: Oceans*, 122, 5952–5969. <https://doi.org/10.1002/2017JC012894>
- Drushka, K., Asher, W. E., Ward, B., & Walesby, K. (2016). Understanding the formation and evolution of rain-formed fresh lenses at the ocean surface. *Journal of Geophysical Research: Oceans*, 121, 2673–2689. <https://doi.org/10.1002/2015JC011527>
- Harkins, W., & Brown, F. (1919). The determination of surface tension (free surface energy), and the weight of falling drops: The surface tension of water and benzene by the capillary height method. *Journal Of The American Chemical Society*, 41(4), 499–524. <https://doi.org/10.1021/ja01461a003>
- Harrison, E. L., & Veron, F. (2017). Near-surface turbulence and buoyancy induced by heavy rainfall. *Journal of Fluid Mechanics*, 830, 602–630. <https://doi.org/10.1017/jfm.2017.602>
- Harrison, E. L., Veron, F., Ho, D. T., Reid, M. C., Orton, P., & McGillis, W. R. (2012). Nonlinear interaction between rain- and wind-induced air-water gas exchange. *Journal of Geophysical Research*, 117, C03034. <https://doi.org/10.1029/2011JC007693>
- Ho, D. T., Bliven, L. F., Wanninkhof, R., & Schlosser, P. (1997). The effect of rain on air-water gas exchange. *Tellus B*, 49(2), 149–158. <https://doi.org/10.1034/j.1600-0889.49.issue.2.3.x>
- Katsafados, P., Varlas, G., Papadopoulos, A., Spyrou, C., & Korres, G. (2018). Assessing the implicit rain impact on sea state during Hurricane Sandy (2012). *Geophysical Research Letters*, 45, 12,015–12,022. <https://doi.org/10.1029/2018GL078673>
- Kudryavtsev, V. N., & Soloviev, A. V. (1990). Slippery near-surface layer of the ocean arising due to daytime solar heating. *Journal of Physical Oceanography*, 20(5), 617–628. [https://doi.org/10.1175/1520-0485\(1990\)020<0617:snsloty2.0.co;2](https://doi.org/10.1175/1520-0485(1990)020<0617:snsloty2.0.co;2)
- Laxague, N. J. M., Curcic, M., Björkqvist, J.-V., & Haus, B. K. (2017). Gravity-capillary wave spectral modulation by gravity waves. *IEEE Transactions on Geoscience and Remote Sensing*, 55(5), 2477–2485. <https://doi.org/10.1109/TGRS.2016.2645539>
- Laxague, N. J. M., Haus, B. K., Bogucki, D. J., & Özgökmen, T. M. (2015). Spectral characterization of fine-scale wind waves using shipboard optical polarimetry. *Journal of Geophysical Research: Oceans*, 120, 3140–3156. <https://doi.org/10.1002/2014JC010403>
- Laxague, N. J. M., Haus, B. K., Ortiz-Suslow, D. G., Smith, C. J., Novelli, G., Dai, H., et al. (2017). Passive optical sensing of the near-surface wind-driven current profile. *Journal of Atmospheric and Oceanic Technology*, 34(5), 1097–1111. <https://doi.org/10.1175/JTECH-D-16-0090.1>
- Laxague, N. J. M., Özgökmen, T. M., Haus, B. K., Novelli, G., Shcherbina, A. Y., Sutherland, P., et al. (2018). Observations of near-surface current shear help describe oceanic oil and plastic transport. *Geophysical Research Letters*, 45, 245–249. <https://doi.org/10.1002/2017GL075891>
- Laxague, N. J. M., & Zappa, C. J. (2020). Observations of mean and wave orbital flows in the ocean's upper centimetres. *Journal of Fluid Mechanics*, 887, A10. <https://doi.org/10.1017/jfm.2019.1019>
- Laxague, N. J. M., Zappa, C. J., LeBel, D. A., & Banner, M. L. (2018). Spectral characteristics of gravity-capillary waves, with connections to wave growth and microbreaking. *Journal of Geophysical Research: Oceans*, 123, 4576–4592. <https://doi.org/10.1029/2018JC013859>
- Lee, T., Fournier, S., Gordon, A. L., & Sprintall, J. (2019). Maritime continent water cycle regulates low-latitude chokepoint of global ocean circulation. *Nature Communications*, 10(1), 2103. <https://doi.org/10.1038/s41467-019-10109-z>
- Millero, F. J., & Poisson, A. (1981). International one-atmosphere equation of state of seawater. *Deep Sea Research Part A, Oceanographic Research Papers*, 28(6), 625–629. [https://doi.org/10.1016/0198-0149\(81\)90122-9](https://doi.org/10.1016/0198-0149(81)90122-9)
- Morton, D., Rudman, M., & Jong-Leng, L. (2000). An investigation of the flow regimes resulting from splashing drops. *Physics of Fluids*, 12(4), 747–763. <https://doi.org/10.1063/1.870332>
- Peirson, W. L., Beyá, J. F., Banner, M. L., Peral, J. S., & Azarmsa, S. A. (2013). Rain-induced attenuation of deep-water waves. *Journal of Fluid Mechanics*, 724, 5–35. <https://doi.org/10.1017/jfm.2013.87>
- Plant, W. J. (1982). A relationship between wind stress and wave slope. *Journal of Geophysical Research*, 87(C3), 1961–1967. <https://doi.org/10.1029/JC087iC03p01961>
- Plant, W. J., & Wright, J. W. (1980). Phase speeds of upwind and downwind traveling short gravity waves. *Journal of Geophysical Research*, 85(C6), 3304. <https://doi.org/10.1029/JC085iC06p03304>
- Poon, Y.-K., Tang, S., Wu, J., Poon, Y.-K., Tang, S., & Wu, J. (1992). Interactions between rain and wind waves. *Journal of Physical Oceanography*, 22(9), 976–987. [https://doi.org/10.1175/1520-0485\(1992\)022<0976:IBRAWWY2.0.CO;2](https://doi.org/10.1175/1520-0485(1992)022<0976:IBRAWWY2.0.CO;2)
- Reynolds, O. (1900). On the action of rain to calm the sea. *Papers on Mechanical and Physical Subject, 1870-1880 Collected Works, vol. 1., 1.*
- Schlüssel, P., Soloviev, A. V., & Emery, W. J. (1997). Cool and freshwater skin of the ocean during rainfall. *Boundary-Layer Meteorology*, 82(3), 439–474. <https://doi.org/10.1023/A:1000225700380>
- Shcherbina, A. Y., D'Asaro, E. A., & Harcourt, R. R. (2019). Rain and sun create slippery layers in the eastern Pacific fresh pool. *Oceanography*, 32(2), 98–107.
- Smeltzer, B. K., Æsoy, E., Ådnøy, A., & Ellingsen, S. Å. (2019). An improved method for determining near-surface currents from wave dispersion measurements. *Journal of Geophysical Research: Oceans*, 124, 8832–8851. <https://doi.org/10.1029/2019JC015202>
- Thompson, E. J., Moum, J. N., Fairall, C. W., & Rutledge, S. A. (2019). Wind limits on rain layers and diurnal warm layers. *Journal of Geophysical Research: Oceans*, 124, 897–924. <https://doi.org/10.1029/2018JC014130>
- Tsimplis, M. N. (1992). The effect of rain in calming the sea. *Journal of Physical Oceanography*, 22(4), 404–412. [https://doi.org/10.1175/1520-0485\(1992\)022<0404:TEORIC>2.0.CO;2](https://doi.org/10.1175/1520-0485(1992)022<0404:TEORIC>2.0.CO;2)
- Tsimplis, M. N., & Thorpe, S. A. (1989). Wave damping by rain. *Nature*, 342(6252), 893–895. <https://doi.org/10.1038/342893a0>
- Turk, D., Zappa, C. J., Meinen, C. S., Christian, J. R., Ho, D. T., Dickson, A. G., & McGillis, W. R. (2010). Rain impacts on CO₂ exchange in the Western Equatorial Pacific Ocean. *Geophysical Research Letters*, 37, L23610. <https://doi.org/10.1029/2010GL045520>
- Varlas, G., Katsafados, P., Papadopoulos, A., & Korres, G. (2018). Implementation of a two-way coupled atmosphere-ocean wave modeling system for assessing air-sea interaction over the Mediterranean Sea. *Atmospheric Research*, 208, 201–217. <https://doi.org/10.1016/j.atmosres.2017.08.019>

- Veron, F., & Melville, W. K. (2001). Experiments on the stability and transition of wind-driven water surfaces. *Journal of Fluid Mechanics*, *446*, 25–65.
- Veron, F., & Mieussens, L. (2016). A kinetic model for particle-surface interaction applied to rain falling on water waves. *Journal of Fluid Mechanics*, *796*, 767–787. <https://doi.org/10.1017/jfm.2016.252>
- Volkov, D. L., Dong, S., Foltz, G. R., Goni, G., & Lumpkin, R. (2019). *Observations of near-surface salinity and temperature structure with dual-sensor Lagrangian drifters during SPURS-2* (Vol. 32). Washington, DC: Oceanography Society.
- Wijesekera, H. W., Paulson, C. A., & Huyer, A. (1999). The effect of rainfall on the surface layer during a westerly wind burst in the Western Equatorial Pacific. *Journal of Physical Oceanography*, *29*(4), 612–632. [https://doi.org/10.1175/1520-0485\(1999\)029<0612:TEOROT>2.0.CO;2](https://doi.org/10.1175/1520-0485(1999)029<0612:TEOROT>2.0.CO;2)
- Wurl, O., Bird, K., Cunliffe, M., Landing, W. M., Miller, U., Mustafa, N. I. H., et al. (2018). Warming and inhibition of salinization at the ocean's surface by cyanobacteria. *Geophysical Research Letters*, *45*, 4230–4237. <https://doi.org/10.1029/2018GL077946>
- Wurl, O., Landing, W. M., Mustafa, N. I. H., Ribas-Ribas, M., Witte, C. R., & Zappa, C. J. (2018). The ocean's skin layer in the tropics. *Journal of Geophysical Research: Oceans*, *124*, 59–74. <https://doi.org/10.1029/2018JC014021>
- Wurl, O., Mustafa, N. I. H., & Ribas-Ribas, M. (2017). *Multiparameter measurement of biochemical properties of the sea surface microlayer in the Pacific Ocean during R/V Falkor cruise FK161010*. Bremen, Germany: PANGAEA. <https://doi.org/10.1594/PANGAEA.882430>
- Yang, Z., Tang, S., Wu, J., Yang, Z., Tang, S., & Wu, J. (1997). An experimental study of rain effects on fine structures of wind waves. *Journal of Physical Oceanography*, *27*(3), 419–430. [https://doi.org/10.1175/1520-0485\(1997\)027<0419:AESORE>2.0.CO;2](https://doi.org/10.1175/1520-0485(1997)027<0419:AESORE>2.0.CO;2)
- Zappa, C. J., Banner, M. L., Schultz, H., Corrada-Emmanuel, A., Wolff, L. B., & Yalcin, J. (2008). Retrieval of short ocean wave slope using polarimetric imaging. *Measurement Science and Technology*, *19*(5), 55,503. <https://doi.org/10.1088/0957-0233/19/5/055503>
- Zappa, C. J., Banner, M. L., Schultz, H., Gemmrich, J. R., Morison, R. P., Lebel, D. A., & Dickey, T. (2012). An overview of sea state conditions and air-sea fluxes during RaDyO. *Journal of Geophysical Research*, *117*, C00H19. <https://doi.org/10.1029/2011JC007336>
- Zappa, C. J., Ho, D. T., McGillis, W. R., Banner, M. L., Dacey, J. W. H., Bliven, L. F., et al. (2009). Rain-induced turbulence and air-sea gas transfer. *Journal of Geophysical Research*, *114*, C07009. <https://doi.org/10.1029/2008JC005008>
- Zappa, C. J., Laxague, N. J. M., Brumer, S. E., & Anderson, S. P. (2019). The impact of wind gusts on the ocean thermal skin layer. *Geophysical Research Letters*, *46*, 11,301–11,309. <https://doi.org/10.1029/2019GL083687>